energies

MDPI

Article

Geochemical Characteristics and Process of Hydrocarbon Generation Evolution of the Lucaogou Formation Shale, Jimsar Depression, Junggar Basin

Wenjun He [1,2], Yin Liu [3,*], Dongxue Wang [2], Dewen Lei [1,2], Guangdi Liu [1], Gang Gao [1], Liliang Huang [1,2] and Yanping Qi [2]

[1] College of Geosciences, China University of Petroleum (Beijing), Beijing 102249, China; fchwj@petrochina.com.cn (W.H.); leidw@petrochina.com.cn (D.L.); lgd@cup.edu.cn (G.L.); gaogang2819@sina.com (G.G.); hlil@petrochina.com.cn (L.H.)

[2] Research Institute of Exploration and Development, Xinjiang Oilfield Company, PetroChina, Urumqi 830013, China; fcwdx@petrochina.com.cn (D.W.); qiyanp@petrochina.com.cn (Y.Q.)

[3] Key Laboratory of Deep Oil and Gas, School of Geosciences, China University of Petroleum (East China), Qingdao 266580, China

* Correspondence: liuyin@upc.edu.cn; Tel.: +86-18366266387

Abstract: Lacustrine shale, represented by the Middle Permian Lucaogou Formation in the Jimsar Depression in the eastern Junggar Basin, has become one of the main areas of shale oil exploration in China. In this study, we used 137 samples of shale from the Lucaogou Formation, drawn from 14 wells in the Jimsar Depression, to investigate their characteristics of pyrolysis, organic carbon and soluble organic matter content, biomarkers, organic microscopic composition, and vitrinite reflectance. Basin simulation and hydrocarbon generation thermal simulation experiments were also conducted in a closed system. The results of this study indicate that the input of an algae source was dominant in the source rocks of the Lucaogou Formation, that the water in which the rocks were deposited had high salinity and strong reducibility, and that the source rocks were oil-prone. The Lucaogou source rocks generally had good hydrocarbon generation capability, but showed significant heterogeneity. At the end of the Cretaceous period, the shales in the Lucaogou Formation entered the oil-generation window as a whole. Currently, the shales of the Lucaogou Formation are generally in the high-maturity stage in the deep part of the depression, producing a large amount of high-maturity oil and condensate gas, while those in the shallow part have relatively low maturity and can only produce a large amount of conventional crude oil. The maximum crude oil generation rate of the Lucaogou Formation shale obtained from the thermal simulation results was 220.2 mg/g of the total organic carbon (TOC), and the maximum hydrocarbon expulsion efficiency was estimated to be 59.3–76.4%.

Keywords: Junggar Basin; Jimsar Depression; shale oil; thermal simulation; source rock evaluation; hydrocarbon generation evolution

Citation: He, W.; Liu, Y.; Wang, D.; Lei, D.; Liu, G.; Gao, G.; Huang, L.; Qi, Y. Geochemical Characteristics and Process of Hydrocarbon Generation Evolution of the Lucaogou Formation Shale, Jimsar Depression, Junggar Basin. *Energies* **2022**, *15*, 2331. https://doi.org/10.3390/en15072331

Academic Editors: Hossein Hamidi

Received: 6 February 2022
Accepted: 21 March 2022
Published: 23 March 2022

1. Introduction

Crude oil and gas exploration in the Junggar Basin began in 1909 and has a history of more than 100 years. As of 2013, the proven crude oil and natural gas reserves in the Junggar Basin were 23.34×10^8 t and 1972×10^8 m^3, respectively [1]. The Junggar Basin is one of the most important onshore oil and gas production sites in China [1,2]. Although the current oil and gas exploration in the Junggar Basin is dominated by conventional reservoirs, the exploration of unconventional shale oil, represented by the Middle Permian Lucaogou Formation (P_2l) in the Jimsar Depression, the Middle Permian Pingdiquan Formation (P_2p) in the Wucaiwan–Shishugou area, and the Lower Permian Fengcheng Formation (P_1f) in Fengcheng area of the northwestern margin, has shown promising results [3–5].

Compared with conventional oil reservoirs, shale oil reservoirs are significantly different, and the main differences are as follows: (1) source–reservoir integration and near-source or intra-source accumulation; (2) extremely low porosity and permeability; (3) the ambiguous boundary conditions of the trap; and (4) Darcy's law of seepage flow not being met during the secondary migration of oil and gas [6–8]. At present, this type of integrated source–reservoir shale oil and gas exploration is still in its infancy in China, and the predicted resource amount is around 11×10^9 t, of which Junggar Basin alone accounts for 29×10^8 t (26.4% of the total) [6]. Unlike foreign shale oil, which is dominated by marine deposits, the shale oil in China is dominated by lacustrine deposits. The source rocks in the lake are typically thick, with a small distribution, and their porosity (<10%) and permeability (<0.1 mD) are lower than those in the maritime environment [6,9]. The P_2l lacustrine source rocks in the Jimsar Depression, located in the eastern part of the Junggar Basin, can be regarded as the world's largest lacustrine mudstone in terms of its thickness and organic matter abundance (Figure 1a,b) [10]. At present, this area is one of the main areas of shale oil exploration in China, with a predicted resource amount of 7.02×10^8 t [1,6].

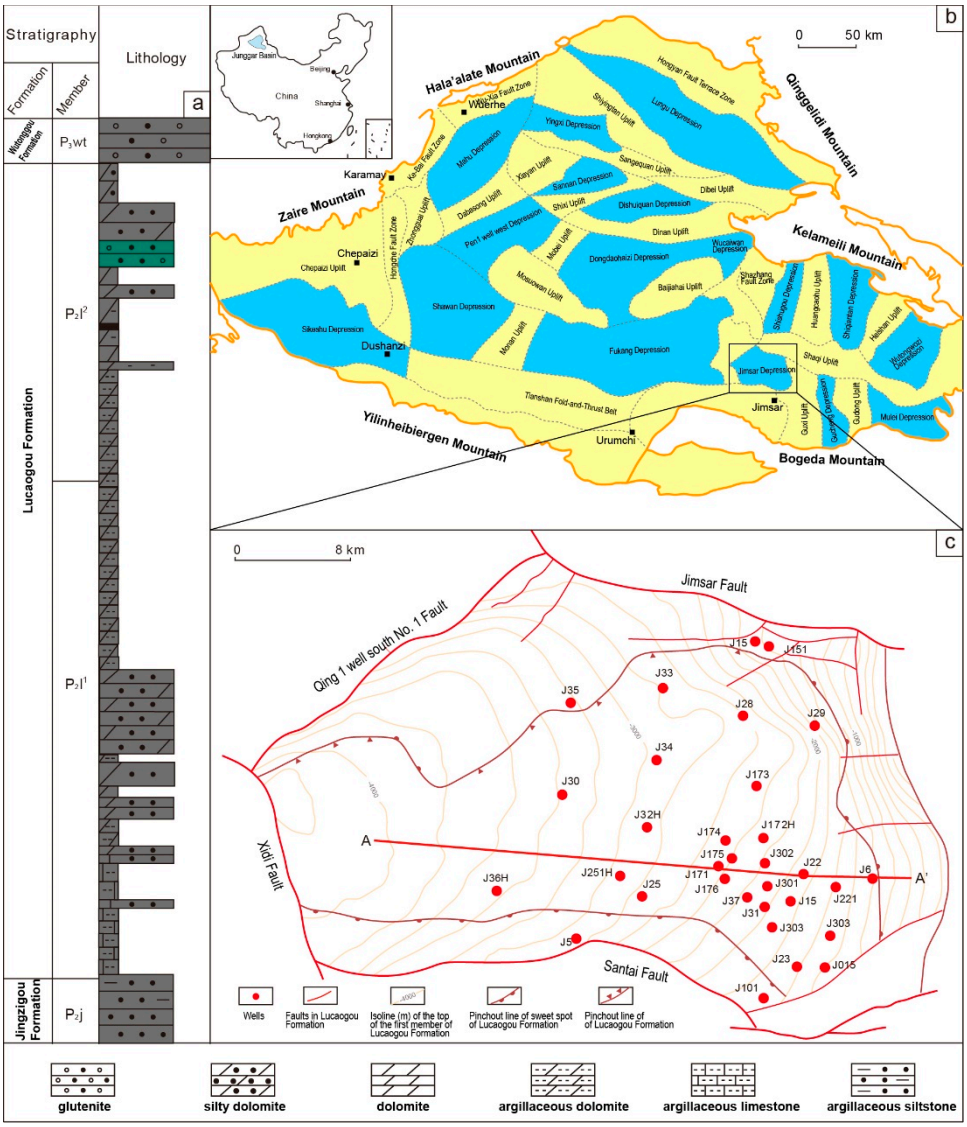

Figure 1. Overview of the petroleum geology of the Jimsar Depression. (**a**) The lithology column of Lucaogou Formation; (**b**) The location of Jimsar Depression in the Junggar Basin; (**c**) Detailed structural map of the Jimsar Depression.

The organic matter abundance and hydrocarbon generation capacity of source rocks are the most important factors used for evaluating the quality of shale oil [8]. Previous researchers had studied P_2l shale oil in the Jimsar Depression, mainly focusing on the sedimentary facies and lithology of the P_2l shale [11], oil and gas source comparison [12], the heterogeneity of the source rocks [13], and the hydrocarbon accumulation process [14,15]. These studies have greatly enriched research on unconventional oil and gas, and promoted the exploration and development of shale oil in the Jimsar Depression. However, current research on the characteristics of hydrocarbon generation and the evolution of P_2l source rocks in the study area is still in a relatively early stage. Based on the analysis of the static hydrocarbon generation capacity of the P_2l source rocks, in this study a gold-tube thermal simulation experiment was conducted in a closed system. Based on this and the two-dimensional basin simulation, the hydrocarbon generation mechanism, hydrocarbon expulsion efficiency, and the evolution process were systematically studied, providing strong support for the evaluation of continental shale oil and gas.

2. Geologic Background

The Junggar Basin is located in the Xinjiang Uygur Autonomous Region in northwestern China, with an area of approximately 1.3×10^5 km^2. It can be divided into a total of six primary structural units, including two major depressions (the Central Depression and the Wulungu Depression), three major uplifts (the Luliang Uplift, the Western Uplift, and the Eastern Uplift), and a thrust-fold belt (the North Tianshan Thrust-Fold Belt) (Figure 1b) [16,17]. The study area is a secondary structural unit in the Eastern Uplift in the Jimsar Depression, bounded by the Shaqi Uplift to the north, the Santai Uplift to the west, the Fukang Fault Zone to the south, and the Guxi Uplift to the east, and has an area of around 1500 km^2 (Figure 1c) [1,18]. The depression has undergone multiple tectonic movements (Hercynian, Indosinian, Yanshanian, and Himalayan movements). There are huge, thick Paleozoic–Cenozoic sedimentary rocks overlying the Precambrian crystalline basement and Paleozoic metamorphic basement. At their thickest, the rocks exceed 5000 m, and the deposits in the depression gradually become thinner from west to east (Figure 1c) [1,17].

The Middle Permian Lucaogou Formation in the Jimsar Depression was formed in a saline lacustrine basin environment after the relict sea was closed [1,19], and it is widely distributed in the depression, with an area of approximately 1278 km^2, a thickness of 200–350 m, and a maximum thickness of >500 m (Figure 1a) [20]. The Lucaogou Formation is a set of lacustrine deposits that has recorded multiple complete cycles of lake water depth fluctuations from shallow to deep, and can be further divided into the upper sub-member (P_2l^2) and the lower sub-member (P_2l^1) (Figure 1a). Previous studies have shown that the Lucaogou Formation contains a set of lacustrine source rocks that are rich in organic matter [15,18,21]. Their lithology includes gray–black mudstone, dolomitic mudstone, siltstone, and dolomite [15,21]. The main lithology of the reservoir includes dolomite, dolomitic siltstone, sandy dolomite, diabase, and a small amount of tuff [11,17]. The storage space of the reservoir is dominated by nanopores and microfractures, the pore throat radius is 100–500 nm, the porosity is 2.5–16.27%, and the permeability is less than 0.1 mD [6].

3. Samples and Analytical Methods

3.1. Samples

In this study, a total of 137 samples of the P_2l source rocks were collected from 14 wells in the Jimsar Depression, including 40 samples from the P_2l^1 member and 97 samples from the P_2l^2 member. The locations of the wells are shown in Figure 1c. Based on these samples, various analytical measurements were carried out on more than 700 samples, including the pyrolysis, extraction, and quantification of the organic carbon and soluble organic matter; the analysis of biomarker compounds; the determination of the whole-rock organic microscopic composition; and the determination of the vitrinite reflectance (Ro).

3.2. Analytical Methods

3.2.1. Evaluation of Source Rocks

The source rock samples were cut into thin sections to observe the lithology of the source rocks and the characteristics of the organic detritus, and determine the Ro. The "Method for Isolation of Kerogen in Sedimentary Rocks", published and implemented in 2003, was used to isolate the kerogen, and the component identification, quantification, and the classification of the kerogen types of the isolated kerogen were carried out based on the "Methods for Microscopic Composition Identification and Type Classification by Transmitted Light-Fluorescence" industry standard (SY/T5125-2014).

The pyrolysis of the source rocks was conducted using a Rock-Eval VI standard pyrolysis instrument (France). The sample was crushed, and 100 mg of the sample was heated in helium gas. The hydrocarbons released during the pyrolysis were monitored using a hydrogen flame ionization monitor, and the CO and CO_2 generated by the heating and oxidation of the residual organic matter after the pyrolysis were detected using a thermal conductivity detector. Following the rock pyrolysis analysis standard (GB/T18602-2012), a constant temperature of 300 °C was set for 3 min to obtain S_1; the temperature was increased from 300 °C to 650 °C at a rate of 25 °C for 1 min to obtain S_2. Then the highest pyrolysis peak temperature (T_{max}), Hydrocarbon Index (HCI), Hydrogen Index (HI), Oxygen Index (OI), Hydrocarbon Generation Potential ($S_1 + S_2$), and Production Index (PI) were obtained through equations for calculating the pyrolysis parameters.

3.2.2. Simulation of Two-Dimensional Basin

The simulation of a two-dimensional basin was carried out using the PetroMod software. The data of heat flows of present and past, and the electrical conductivity of the source rocks, were obtained from previous studies that had carried out simulations [22,23]. The solution (EasyRo) given by Sweeney and Burnham (1990) [24] was used to convert the result to source rock maturity, and the applicable maturity interval was 0.3–4.6% Ro.

3.2.3. Thermal Simulation Experiment in a Closed System

The source rock sample was sealed in a gold tube under the protection of an argon gas atmosphere. The gold tube was placed in an autoclave, and the autoclave was filled with water using a high-pressure pump. The high-pressure water caused the gold tube to be flexibly deformed, thereby exerting pressure on the sample. The sample was sealed under the protection of argon to ensure that there was no air contamination. The gold tube was sealed via arc welding. The samples were heated at rates of 20 °C/min and 2 °C/min. The temperature difference between each autoclave was less than 1 °C. The pressure was 50 MP, and the pressure fluctuation was less than 1 MP. The temperature range was 150–456 °C, and the temperature fluctuation was less than 1 °C. After heating, the gold tube was removed from the autoclave. The detected contents were gas (C_1–C_4), light hydrocarbons (C_6–C_{14}), and heavy hydrocarbons (C_{14+}).

4. Results and Discussion

4.1. Depositional Environment of Source Rocks

4.1.1. Normal Alkanes and Isoprenoid Alkanes

Isoprenoid alkane compounds are commonly used as indicators of the sedimentary environment [25,26]. The pristane/phytane (Pr/Ph) ratios of the P_2l source rocks in the Jimsar Depression were 0.81–2.62, with an average of 1.37. Most of the values were in the range of 0.75–1.5, but quite a few samples had values of >2 (Table 1). Peters et al. (2005) [25] pointed out that when the Pr/Ph ratio is 0.8–3.0, there is great uncertainty in using this ratio to explain the depositional environment of the source rock. Therefore, the ratio of isoprenoid to normal alkanes [27] was used in this study. As is shown in Figure 2, the Pr/*n*-C_{17} and Ph/*n*-C_{18} values were 0.14–6.40 (average 1.54) and 0.09–4.33 (average 1.43), respectively, indicating a reducing environment overall, with bacteria and algae as the main sources of organic matter. The contribution of land-based organic matter was low,

and the maturity was not high. It should be noted that the distribution characteristics of the isoprenoid alkanes and *n*-alkanes are also controlled by their maturity [25,28]. The maturity of the samples from the study area was relatively low, so the impact of the maturity could generally be ignored (Table 1, Figure 2).

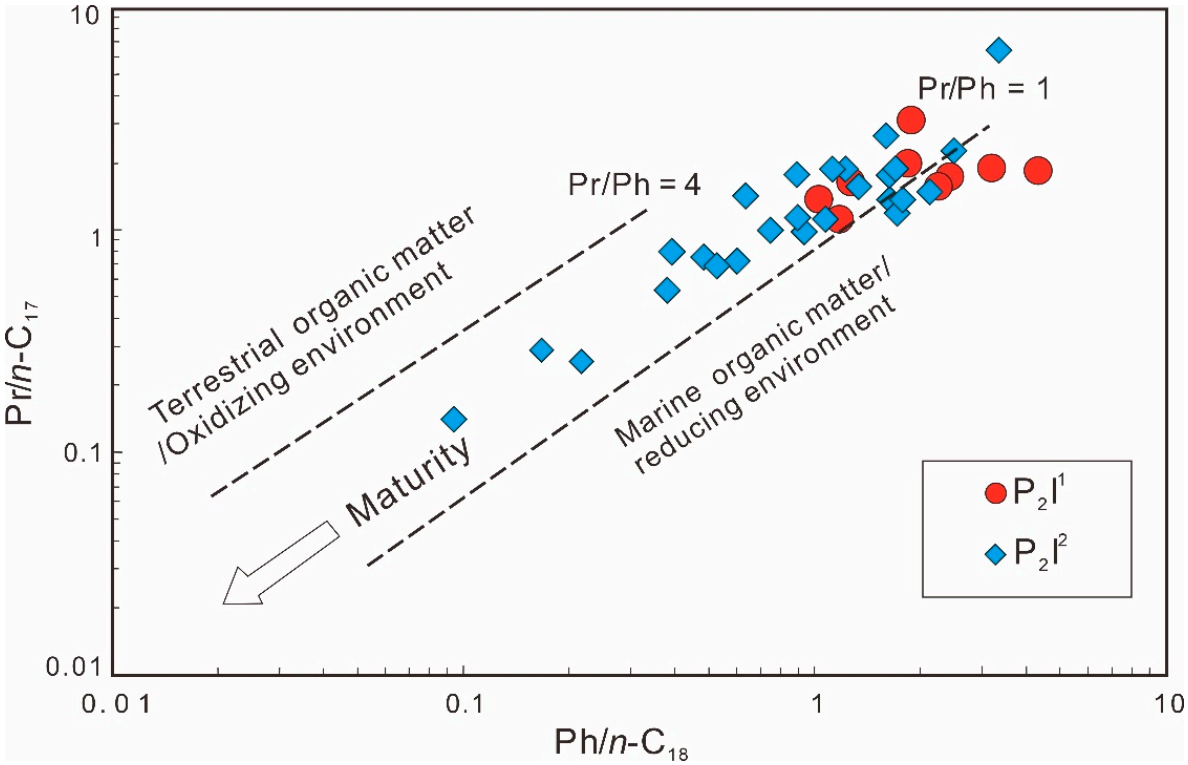

Figure 2. Plot of Pr/*n*-C_{17} vs. Ph/*n*-C_{18} showing the depositional environment of the P_2l source rocks in the Jimsar Depression (modified after Shanmugam, 1985) [27] (terrestrial organic matter/oxidation environment; maturity; marine organic matter/reducing environment).

Table 1. Biomarker fingerprints of P_2l shale in the Jimsar Depression.

Well	Depth(m)	Strata	Lithology	C_{19}/C_{21}-Tricyclic Terpane	Tricyclic Terpane/Pentacyclic Terpane	C_{24}-Tetracyclic Terpane/C_{26}-Tricyclic Terpane	$C_{35}/(C_{31}–C_{35})$ Homohopane %	$C_{30}\alpha\beta$-Hopane/$C_{29}\alpha\alpha\alpha$,(R + S)-Sterane	Gammacerane Index	C_{31R}/C_{30}-Hopane	Ts/(Ts + Tm)	C_{27}-Sterane (%)	C_{28}-Sterane (%)	C_{29}-Sterane (%)
Ji15	2280.63	P_2l^1	Dark gray fluorescent mudstone	0.41	0.29	1.12	7.07	6.79	0.23	0.10	0.43	23.78	23.77	52.46
Ji174	3218.97	P_2l^1	Dark gray calcareous mudstone	0.12	0.12	1.95	2.72	4.85	0.28	0.12	0.05	13.80	37.24	48.96
Ji174	3227.14	P_2l^1	Dark gray dolomitic mudstone	0.13	0.13	1.55	2.66	6.59	0.31	0.17	0.04	14.81	37.11	48.09
Ji24	1691.75	P_2l^1	Gray black mudstone	0.08	0.07	0.62	2.87	5.58	0.31	n.d.	0.27	18.41	32.77	48.83
Ji17	3138.01	P_2l^2	Black gray mudstone	0.10	0.14	1.06	4.16	8.20	0.28	0.11	0.09	14.99	35.39	49.62
Ji17	3138.01	P_2l^2	Black gray mudstone	0.10	0.05	0.82	4.01	12.73	0.36	0.16	0.32	34.81	26.13	39.06
Ji17	3135.33	P_2l^2	Gray black mudstone	0.13	0.06	1.40	3.79	9.88	0.39	0.22	0.33	36.51	26.17	37.33
Ji17	3135.33	P_2l^2	Gray black mudstone	0.07	0.04	0.71	4.05	19.28	0.35	0.15	0.29	42.15	22.16	35.70
Ji174	3135.31	P_2l^2	Dark gray mudstone	0.12	0.15	1.28	2.40	4.62	0.34	0.12	0.07	20.25	34.09	45.66
Ji174	3113.3	P_2l^2	Dark gray mudstone	0.10	0.16	1.46	2.57	4.08	0.42	0.22	0.10	18.88	33.39	47.73
Ji174	3134.05	P_2l^2	Black gray mudstone	0.08	0.10	1.38	2.70	5.44	0.35	0.20	0.10	22.94	31.56	45.50
Ji174	3146.16	P_2l^2	Dark gray mudstone	0.12	0.18	1.65	2.90	3.39	0.19	n.d.	0.12	18.53	41.45	40.01
Ji174	3158.88	P_2l^2	Dark gray mudstone	0.32	0.04	8.93	2.56	6.01	0.21	0.18	0.23	19.84	39.07	41.10
Ji174	3166.74	P_2l^2	Dark gray mudstone	0.11	0.21	2.42	2.23	3.02	0.27	0.17	0.16	21.47	40.29	38.24
Ji174	3177.55	P_2l^2	Dark gray mudstone	0.16	0.09	3.62	2.13	6.44	0.12	0.12	0.25	22.08	37.87	40.05
Ji174	3217.51	P_2l^2	Dark gray calcareous mudstone	0.12	0.17	1.30	2.80	4.89	0.31	0.11	0.06	13.10	35.79	51.11
Ji174	3130.76	P_2l^2	Black gray mudstone	0.12	0.12	2.29	2.32	8.37	0.26	0.16	0.14	25.81	30.83	43.36
Ji174	3114.73	P_2l^2	Dark gray mudstone	0.11	0.16	1.37	2.39	7.26	0.39	0.20	0.14	31.83	28.72	39.45
Ji174	3117.75	P_2l^2	Dark gray mudstone	0.13	0.15	1.96	2.45	11.13	0.41	n.d.	0.10	20.59	32.54	46.88
Ji174	3118.78	P_2l^2	Dark gray mudstone	0.14	0.19	2.15	2.04	7.08	0.38	0.19	0.09	17.65	34.22	48.13
Ji174	3122.14	P_2l^2	Dark gray mudstone	0.18	0.09	5.37	3.39	4.14	0.31	0.19	0.17	15.76	31.31	52.93

Table 1. *Cont.*

Well	Depth(m)	Strata	Lithology	C_{19}/C_{21}-Tricyclic Terpane	Tricyclic Terpane/Pentacyclic Terpane	C_{24}-Tetracyclic Terpane/C_{26}-Tricyclic Terpane	$C_{35}/(C_{31}–C_{35})$ Homohopane %	$C_{30}\alpha\beta$-Hopane/$C_{29}\alpha\alpha\alpha$,(R + S)-Sterane	Gammacerane Index	C_{31R}/C_{30}-Hopane	Ts/(Ts + Tm)	C_{27}-Sterane (%)	C_{28}-Sterane (%)	C_{29}-Sterane (%)
Ji174	3146.19	P_2l^2	Dark gray mudstone	0.12	0.16	1.11	3.66	2.80	0.12	0.20	0.11	19.22	44.60	36.19
Ji174	3152.98	P_2l^2	Dark gray mudstone	0.18	0.21	4.31	2.94	6.27	0.27	0.18	0.12	14.69	52.95	32.36
Ji174	3155.32	P_2l^2	Dark gray dolomitic mudstone	0.22	0.10	8.54	1.46	5.91	0.26	0.21	0.15	14.69	57.26	28.05
Ji174	3162.02	P_2l^2	Dark gray mudstone	0.22	0.03	7.27	2.34	7.27	0.25	0.18	0.22	18.76	41.56	39.68
Ji174	3196.3	P_2l^2	Dark gray dolomitic mudstone	0.09	0.16	1.55	2.44	7.47	0.27	0.16	0.18	20.70	37.28	42.02
Ji22	2543.06	P_2l^2	Dark gray mudstone	0.10	0.15	1.69	1.75	5.25	0.35	0.13	0.12	23.97	33.63	42.40
Ji22	2554.54	P_2l^2	Dark gray dolomitic mudstone	0.06	0.13	0.87	2.44	6.56	0.40	0.08	0.08	23.69	30.96	45.35
Ji22	2552.67	P_2l^2	Dark gray dolomitic mudstone	0.09	0.09	2.39	1.51	5.97	0.25	0.08	0.21	35.35	32.11	32.54
Ji22	2554.8	P_2l^2	Dark gray dolomitic mudstone	0.08	0.07	1.76	2.35	10.36	0.55	0.22	0.10	33.07	33.13	33.80
Ji23	2296.12	P_2l^2	Gray black calico mudstone	0.05	0.07	0.81	2.59	8.57	0.51	0.21	0.21	31.11	30.44	38.46
Ji23	2296.04	P_2l^2	Gray black mudstone	0.04	0.06	0.61	2.48	8.32	0.50	0.21	0.22	30.02	30.41	39.57
Ji5	3535.56	P_2l^2	Gray black mudstone	1.43	0.08	n.d.	n.d.	4.73	0.37	0.25	0.52	17.43	32.51	50.06
Ji7	2059	P_2l^2	Gray black mudstone	0.16	0.05	1.26	4.76	1.72	0.16	0.21	0.30	17.42	17.36	65.22
Ji7	1949.61	P_2l^2	Gray black mudstone	0.05	0.08	1.19	6.70	1.26	0.24	0.17	0.24	18.73	31.91	49.36
Ji7	2069.99	P_2l^2	Dolomitic mudstone	0.29	0.19	n.d.	n.d.	2.10	0.13	0.23	0.09	32.46	31.15	36.39
Ji7	2160.2	P_2l^2	Dolomitic mudstone	0.13	0.12	3.62	3.62	2.50	0.24	0.25	0.34	24.89	31.31	43.79
Ji7	2287.45	P_2l^2	Dolomitic mudstone	0.09	0.17	1.06	2.75	1.29	0.14	n.d.	0.35	22.83	17.69	59.47
Ji7	1949.61	P_2l^2	Dark gray dolomitic mudstone	0.00	0.08	1.17	7.19	2.16	0.25	0.21	0.26	19.69	33.79	46.52
Ji7	2160.2	P_2l^2	Dark gray dolomitic mudstone	0.24	0.05	10.90	n.d.	8.14	0.23	0.13	0.37	29.38	30.63	39.99
Ji7	2287.45	P_2l^2	Dark gray dolomitic mudstone	0.33	0.06	2.80	3.06	9.21	0.20	n.d.	0.10	32.70	26.05	41.25
Ji7	2069	P_2l^2	Black mudstone	0.07	0.08	0.86	n.d.	1.51	0.27	n.d.	0.21	17.61	28.06	54.33
Ji7	2160	P_2l^2	Black dolomitic mudstone	0.15	0.06	1.86	5.31	4.14	0.61	n.d.	0.28	16.64	23.63	59.73

4.1.2. Terpanes

Tricyclic terpanes are abundant in the P_2l shale of the study area, mainly in the range of C_{19}–C_{28} (Figure 3), indicating that their formation was closely related to the input of an algae source [29]. The baseline of the GC–MS spectra is nearly horizontal, with no UCM "hump", suggesting that there was nearly no influence of biodegradation. The source rocks are rich in hopanes. The $C_{30}\alpha\beta$-hopane/$C_{29}\alpha\alpha\alpha$,(R + S)-sterane ratios are 1.26–19.28, with an average of 6.12 (Figure 3, Table 1), suggesting that bacteria reproduced rapidly in a lake environment and provided a large amount of hopane precursors. The ratios of some individual samples were relatively low, which may be related to a certain amount of terrestrial organic matter input. C_{31}–C_{35} homohopanes are closely related to prokaryotic microorganisms, and high abundance of C_{35} homohopane often indicates a strongly reducing depositional environment [25,30]. The C_{35} homohopane index (C_{35}/(C_{31}–C_{35}) homohopane%) of the P_2l shale is relatively high, with a range of 1.46–7.19 and an average of 3.17, indicating that the sedimentary water body had strong reducibility (Figure 3, Table 1). The C_{31}R homohopane/C_{30} hopane ratios are 0.08–0.25, with an average of 0.17, also exhibiting the characteristics of lacustrine crude oil (Figure 3, Table 1). Gammacerane can effectively reflect the stratification of sedimentary water bodies, which in turn is related to the salinity of the water body [31]. The abundance of gammacerane in coal-measure source rocks formed in a swamp environment is very low, and their gammacerane index (Gammacerane/(Gammacerane + $C_{30}\alpha\beta$-hopane)) is usually less than 0.05 (or even less than 0.01). The abundance of gammacerane in lacustrine sedimentary mudstone is relatively high, and the gammacerane index is greater than 0.05 in most cases [31,32]. The gammacerane index values of P_2l shale source rocks in the study area were 0.12–0.61, with an average of 0.30 (Figure 3, Table 1), indicating that evaporation was very strong and the sedimentary water body had a fairly high salinity. In other words, in the Middle Permian, the Jimsar Depression was a saline lake basin.

Table 2. The definition of the biomarker code.

Code	Name	Code	Name
S1	5α(H),14β(H)-pregnane	T6	C24,13β(H),14α(H)-tricyclic terpane
S2	C22-homopregnane	T7	C25,13β(H),14α(H)-tricyclic terpane
S3	20S-ααα-sterane	T8	C26-tricyclic terpane
S4	20R-αββsterane	T9	C26-tricyclic terpane
S5	20S-αββ-sterane	T10	C24-tetracyclic terpane
S6	20R-ααα-sterane	T11	C28-tricyclic terpane
S7	20R-24-ethyl-10α13β17α-rearranged sterane	T12	C28-tricyclic terpane
S8	20S-24-ethyl-10α13α17β-rearranged sterane	T13	18α,-22,29,30-trisnorhopane(Ts)
S9	20S-24-methyl-ααα-sterane	T14	17α,-22,29,30-trisnorhopane(Tm)
S10	20R-24-methyl-αββ-sterane	T15	17α,21β-30-norhopane
S11	20S-24-methyl-αββ-sterane	T16	17α(H),21β(H)-hopane
S12	20R-24-methyl-ααα-sterane	T17	17β(H),21α(H)-moretane
S13	20S-24-ethyl-ααα-sterane	T18	22S-17α(H),21β(H)-homohopane
S14	20R-24-ethyl-αββ-sterane	T19	22R-17α(H),21β(H)-homohopane
S15	20S-24-ethyl-αββ-sterane	T20	Gammacerane
S16	20R-24-ethyl-ααα-sterane	T21	22R-17β(H),21α(H)-homohopane

Table 2. *Cont.*

Code	Name	Code	Name
T1	C19,14β(methyl)-tricyclic terpane	T22	22S-17α(H),21β(H)-double homohopane
T2	C20,13β(H),14α(H)-tricyclic terpane	T23	22R-17α(H),21β(H)-double homohopane
T3	C21,13β(H),14α(H)-tricyclic terpane	T24	22S-17α(H),21β(H)-trishomohopane
T4	C22,13β(H),14α(H)-tricyclic terpane	T25	22R-17α(H),21β(H)-trishomohopane
T5	C23,13β(H),14α(H)-tricyclic terpane		

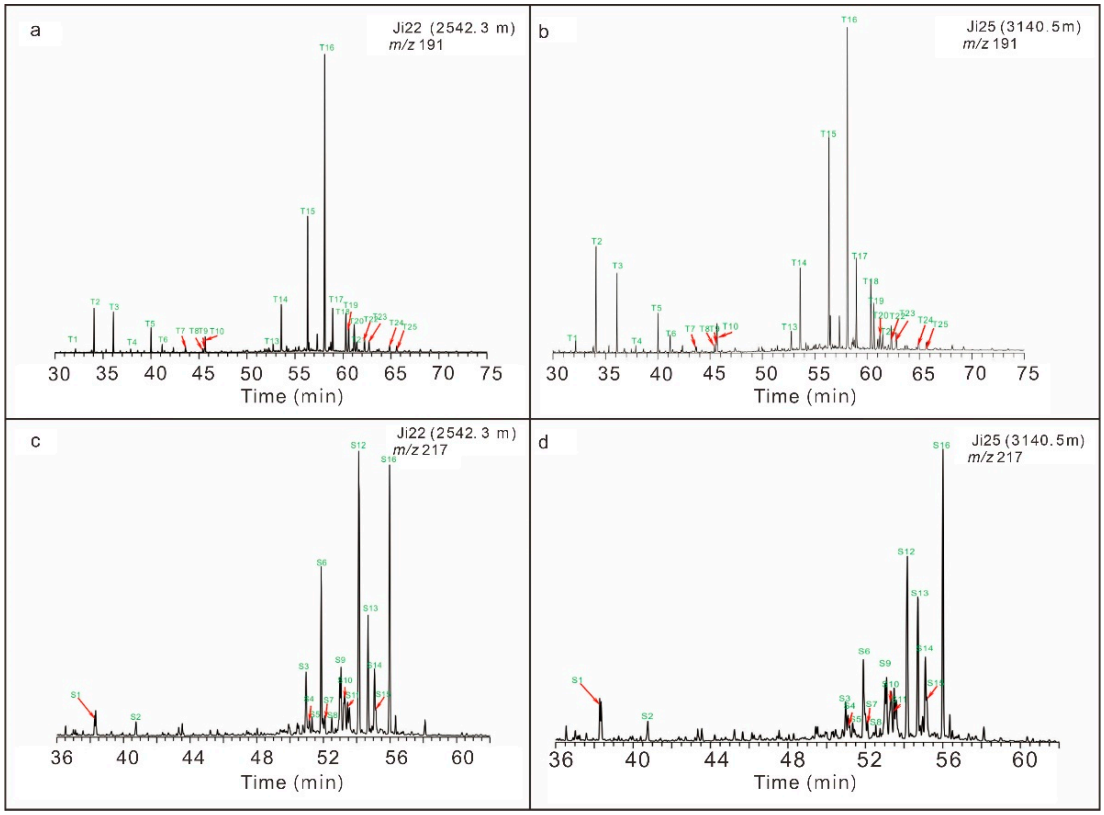

Figure 3. Gas chromatography–mass spectroscopy (GC–MS) spectra of the biomarkers of the (**a**,**b**) terpanes (*m*/*z* 191) and (**c**,**d**) steranes (*m*/*z* 217) in the P_2l source rocks in the Jimsar Depression (the compounds corresponding to all of the labels are shown in Table 2).

4.1.3. Sterane

The data suggest that the Lucaogou source rocks were rich in C_{27} and C_{28} steranes, implying the existence of large quantities of algae organic matter [33]. The contents of the C_{27}, C_{28}, and C_{29} regular steranes in the P_2l shale in the study area were 13.1–42.2% (average 22.9%), 17.4–57.3% (average 33.0%), and 28.1–57.3% (average 44.1%), respectively (Table 1, Figures 3 and 4). The total content of the C_{27} and C_{28} regular steranes in the source rock samples exceeded the content of C_{29} regular steranes. This indicates that algae organic matter was dominant; however, it also indicates that there may have been some contribution from terrestrial organic matter to source rocks in the study area. The relatively high C_{29} sterane content was not just related to the source of the organic matter; it was also affected by the depositional environment of the source rocks. Generally, lacustrine source rocks dominated by input of algae sources have higher relative C_{29} sterane content than marine carbonate/shale [34–36]. Overall, the P_2l shale had relatively high C_{27} and C_{28} sterane content (Figure 4).

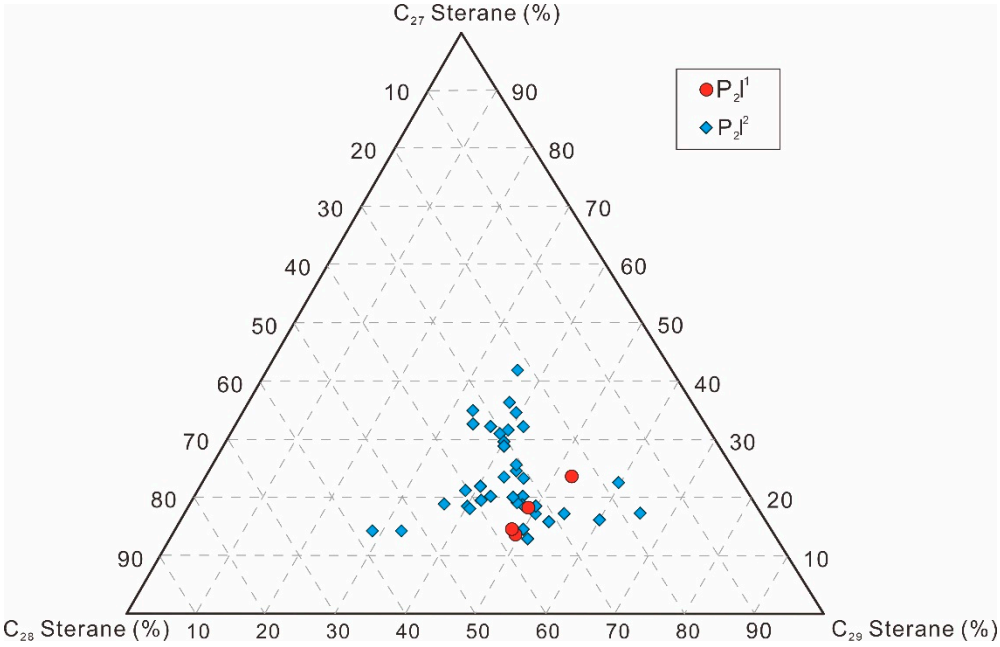

Figure 4. Ternary diagram of the relative percentages of the C_{27}, C_{28}, and C_{29} regular steranes in the P_2l source rocks in the Jimsar Depression.

4.2. Type and Abundance of Source Rocks

4.2.1. Types of Organic Matter

The elemental analysis revealed that the H/C atomic ratios of the P_2l^1 member in the study area were 0.79–1.33 (average 1.06); the O/C atomic ratios were 0.04–0.08 (average 0.06); the H/C atomic ratios of the P_2l^2 member were 0.82–1.60 (average 1.23); the O/C atomic ratios were 0.03–0.30 (average 0.08); and the two sets of source rocks did not exhibit significant differences, mainly exhibiting the characteristics of type II kerogen (Figure 5a). Hunt (1996) [37] pointed out that when the H/C atomic ratio is >0.8, organic matter starts to have the capability to generate oil. According to this standard, the P_2l shale had a relatively high H/C atomic ratio and was a set of oil-prone source rocks. It should be noted that large differences in the H/C atomic ratios of the different samples indicated that this set of source rocks was strongly heterogeneous.

Based on the pyrolysis HI values of >600, 300–600, 200–300, 50–200, and <50 mg hydrocarbons/g TOC, the organic matter can be divided into five types: type I (extremely oil-prone type), type II (oil-prone type), II/III type (oil/gas-prone type), type III (gas-prone type), and type IV (non-source rock) (Figure 5b) [38,39]. The HI values of the P_2l^1 member in the study area were 12–781 mg hydrocarbons/g TOC (average of 367 mg hydrocarbons/g TOC), the HI values of the P_2l^2 member were 72–808 mg hydrocarbons/g TOC (average of 390 mg hydrocarbons/g TOC), and there was no large difference between the two sets of source rocks (Figure 5b). The type I, type II, type II/III, type III, and type IV samples accounted for 14.5%, 47.1%, 21.0%, 15.2%, and 2.0% of the total samples, respectively, indicating that the P_2l source rocks were dominated by type II kerogen, and that type I kerogen did not account for a large proportion. In addition, this set of source rocks was very strongly heterogeneous, and the types of parent materials involved were very different. This heterogeneity was very obvious even in samples from the same well. As an example, for Well Ji174, from which a large number of samples were collected, the HI values of the P_2l^1 and P_2l^2 members were 48–294 and 72–808 mg hydrocarbons/g TOC, respectively.

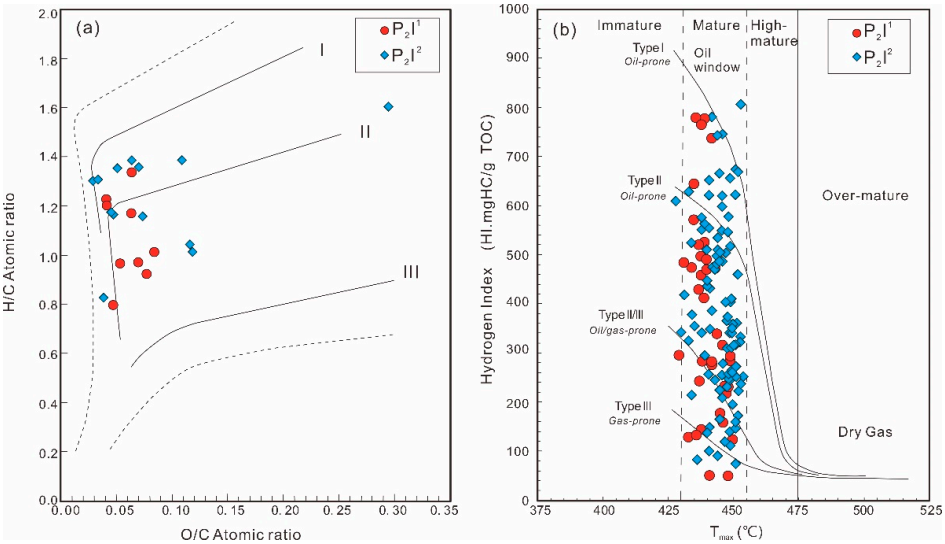

Figure 5. Plots of (**a**) O/C vs. H/C and (**b**) atomic ratio of HI vs. T_{max} showing the organic matter types of the P_2l source rocks in the Jimsar Depression (H/C, atomic ratio; O/C, atomic ratio; immature; mature; oil generation window; highly mature; condensate oil-wet gas; over-mature; dry gas generation).

The analysis of the organic microscopic compositions of whole-rock samples revealed that the contents of the vitrinite group and exinite group of the P_2l source rocks were low (<20%), while the contents of the sapropelinite group + exinite group were very high (62.3–78.7%). In general, the sapropelinite group component mainly generated crude oil, the vitrinite group component mainly generated natural gas, the exinite group component generated both, and the inertinite group component had almost no potential for hydrocarbon generation. Therefore, the P_2l source rocks in the study area should mainly be oil-generating. Figure 6 shows the results of the whole-rock organic microscopic composition analysis of a core sample (2321.4 m) of P_2l^1 from Well Ji15. Under reflected fluorescence, the clay (Cl) substrate exhibited a strong fluorescence, and, among them, the parallel-distributed microsporinite (MiS), resinite (R), liptodetrinite (Ld), and vitrodetrinite (Cd) were also widely distributed (Figure 6). Under reflected plane-polarized light (oil immersion), the clay (Cl) minerals exhibited a granular structure in which Cd and semifusinite (SF) fragments were distributed and the latter's structure was broken. Pyrite (Py) was widely distributed, reflecting the strong reducibility of the sedimentary environment and the good organic matter preservation conditions (Figure 6).

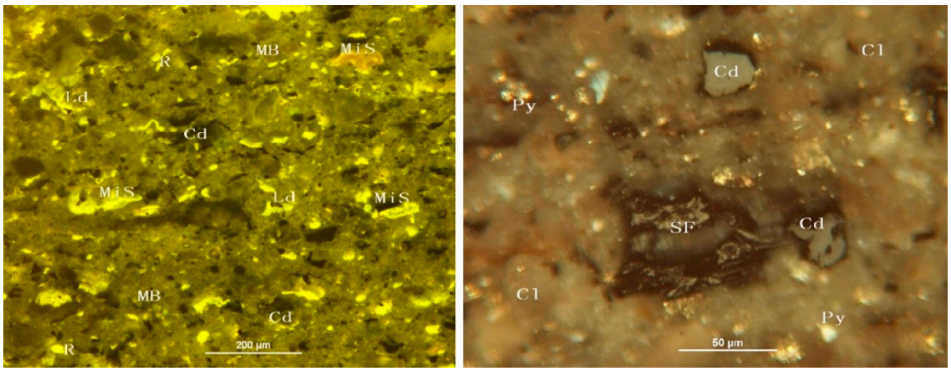

Figure 6. Analysis of the organic microscopic composition of the whole-rock P_2l^1 sample (2321.4 m) from Well Ji15 (left image: reflected fluorescence; right image: reflected plane-polarized light). Cl is clay; MiS is microsporinite; R is resinite (R); Ld is liptodetrinite; Cd is vitrodetrinite; SF is semifusinite; MB is mineral bitumen; Py is pyrite.

4.2.2. Abundance of Organic Matter

Huang et al. (1982) [40] summarized the abundance of organic matter in the source rocks of the main petroliferous basins in China, and proposed corresponding evaluation criteria for lacustrine source rocks deposited in freshwater and brackish water environments (Figure 7). The TOC values of the P_2l^1 and P_2l^2 source rocks were 0.38–7.55% (average 3.30%) and 0.34–12.45% (average 3.80%), respectively. From the perspective of organic carbon, the proportions of good and extremely good source rocks in the P_2l^1 source rocks were 15.0% and 70.0%, respectively, while the proportions of good and extremely good source rocks in the P_2l^2 source rocks were 14.3% and 75.5%, respectively. The source rock $S_1 + S_2$ values of the P_2l^1 and P_2l^2 members were 0.26–39.44 mg hydrocarbons/g rock (average of 15.21 mg hydrocarbons/g rock) and 0.47–78.96 mg hydrocarbons/g rock (average of 17.60 mg hydrocarbons/g rock), respectively (Figure 7). In terms of $S_1 + S_2$, the proportions of the good and extremely good source rocks in the P_2l^1 member were 40% and 30%, respectively, while the proportions of the good and extremely good source rocks in the P_2l^2 source rocks were 37.8% and 34.7%, respectively (Figure 7).

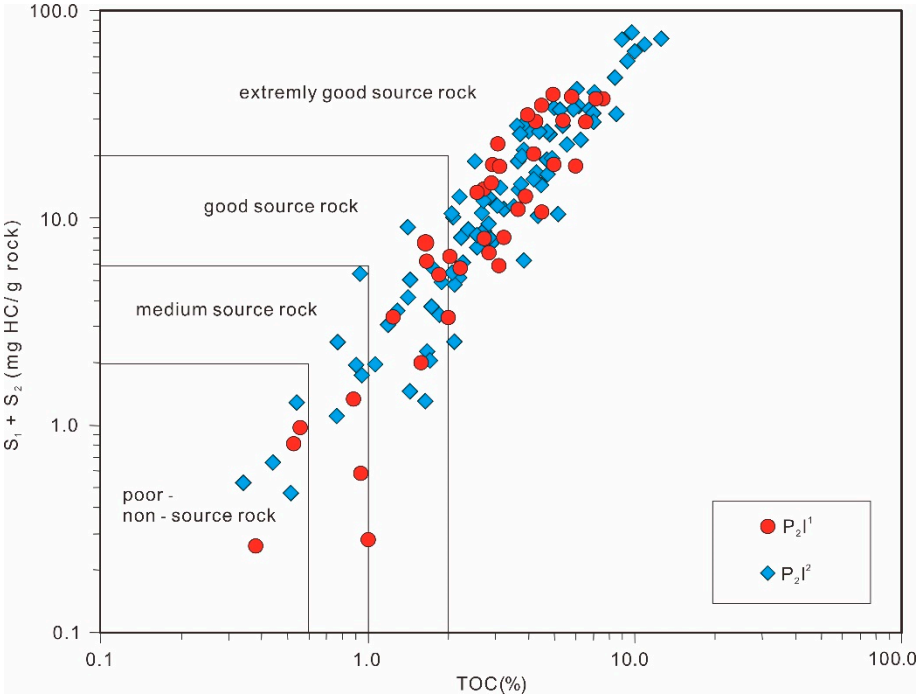

Figure 7. TOC vs. $S_1 + S_2$ diagram showing the abundance of organic matter in the P_2l source rocks in the Jimsar Depression (extremely good source rock; good source rock; medium-grade source rock; poor-non-source rock).

From the perspective of the TOC and $S_1 + S_2$, the P_2l source rocks were generally good to extremely good source rocks, but they also exhibited a strong heterogeneity (Figure 7). It should be noted that when the TOC was used as the evaluation standard, the quality of the source rocks was considerably better than the results obtained using the hydrocarbon generation potential as the standard. For example, when TOC was used as the evaluation criterion, the proportion of extremely good source rocks out of the total number of samples was twice as high as the results obtained based on $S_1 + S_2$. This is mainly due to the difference in the hydrogen content of the source rocks. In thermochemical reactions, carbon must be combined with hydrogen to generate hydrocarbons. If the hydrogen content is low, even if the organic carbon content is high, the result is often ineffective. The heterogeneity of the hydrogen content of the source rocks, which is reflected in the analysis of organic elements and the pyrolysis hydrogen index, also confirms this view (Figure 5). When

evaluating the P_2l source rocks, the results obtained using the pyrolysis hydrocarbon generation potential as the standard may be more reliable.

4.3. Thermal Evolution of the Source Rocks

4.3.1. Maturity of the Source Rocks

The vitrinite reflectance values of the P_2l source rocks in the study area were 0.52–1.24%, with an average of 0.71%, meaning they were within the main oil generation window. It is generally believed that when S_2 is less than 0.2 mg hydrocarbons/g rock, T_{max} is unreliable [41]. Except for the two samples from Well Ji5, the S_2 values of the samples from the study area were greater than 0.2 mg hydrocarbons/g rock. The T_{max} values obtained based on these values were generally reliable, ranging from 428 °C to 454 °C, with an average of 445 °C. The samples were essentially in a mature stage, which is consistent with the situation reflected by the vitrinite reflectance.

The gas chromatographic analysis of the extracted source-rock bitumen revealed that the carbon preference index (CPI) values of the P_2l source rocks in the Jimsar Depression were 1.18–2.0 (average 1.41), and the odd-to-even preference (OEP) was 1.14–1.71 (average 1.30), exhibiting a significant odd–even predominance, which indicates that the maturity of the source rocks was not high. The C_{29}20S/(S + R)-sterane and $C_{29}\beta\beta/(\alpha\beta\beta + \alpha\alpha\alpha)$-sterane ratios of the source rock extracts were 0.09–0.46 and 0.11–0.45, respectively, making them lower than the equilibrium values (0.67–0.71 and 0.52–0.55), though they were still within the oil generative window (Figure 8, Table 1) [25].

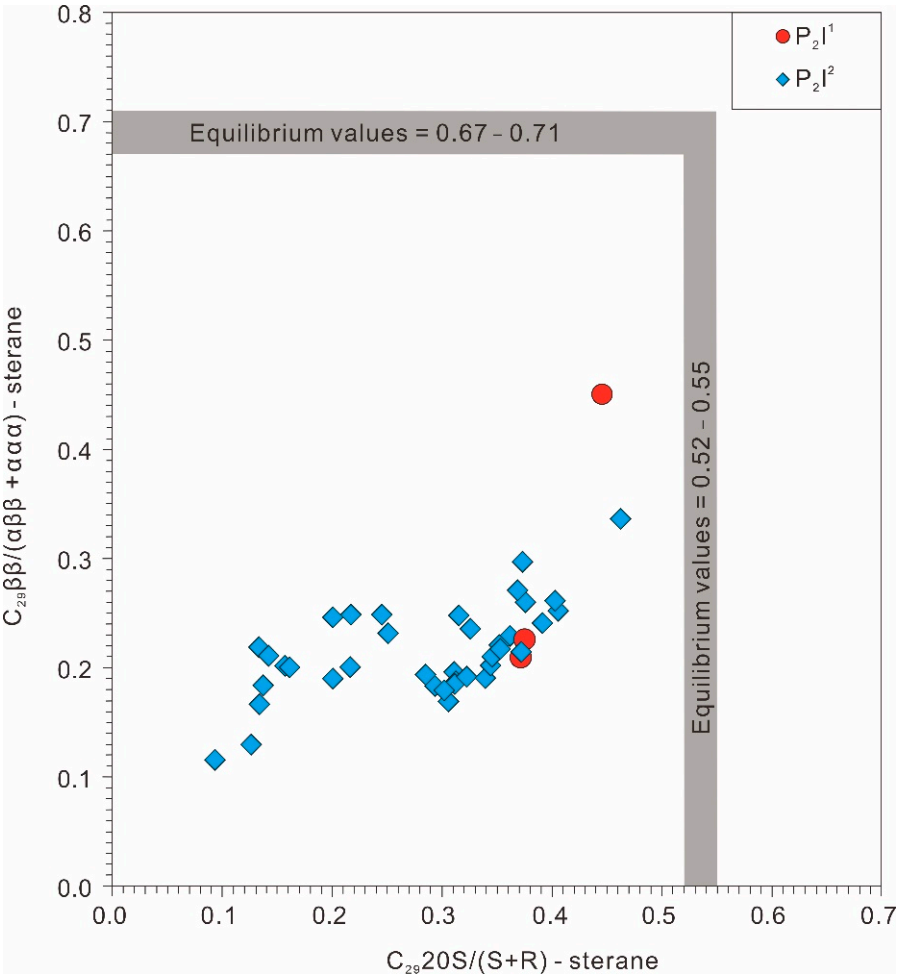

Figure 8. Use of sterane isomer maturity parameters to determine the organic matter maturity of the P_2l source rocks in the Jimsar Depression.

4.3.2. Thermal Evolution of the Source Rocks

Based on a two-dimensional seismic profile crossing the Jimsar Depression in the east–west direction, we restored the hydrocarbon generation and expulsion history and burial history of the P_2l source rocks (Figure 9; the location of the profile is shown in Figure 1c). At the end of the Triassic, the maturity of the P_2l shale was low, EasyRo < 0.5%, and it had not yet reached the oil generation threshold (Figure 9a). The maturity of the P_2l shale increased significantly at the end of the Cretaceous, with an EasyRo > 0.7%, and it entered the main oil generation window, producing a large amount of normal crude oil. The highly mature stage (1.0–1.3% EasyRo) was reached in the deep part of the Depression, and certain amounts of highly mature crude oil and condensate gas were generated (Figure 9b). After the Cretaceous deposition, the formation was uplifted and denuded, and the hydrocarbon generation process in the P_2l source rocks stalled (Figure 9c). In the Paleogene, P_2l continued to settle (Figure 9d). Currently, the deep part of the depression has generally reached the high-maturity stage, producing a large amount of highly mature oil and condensate gas (1.0–1.3% Ro). The shallow part had relatively low maturity and could only generate a large amount of normal crude oil (0.7–1.0% EasyRo) (Figure 9e).

4.4. Thermal Simulation Experiment on Source Rocks in a Closed System

In this study, a P_2l calcareous and siliceous black shale sample (core, 2321.4 m; sampling location is shown in Figure 1c) from Well Ji15 in the eastern margin of the Jimsar Depression was selected. Its kerogen was extracted, and a gold-tube thermal simulation experiment was carried out in a closed system. The total organic carbon content of this sample was 2.46%, the hydrocarbon generation potential ($S_1 + S_2$) was 13.36 mg hydrocarbons/g rock, and the HI was 491 mg/g TOC. Generally speaking, the abundance index was in the middle of the range of the P_2l shales in the Jimsar Depression, and was representative. In addition, the maturity of the sample was relatively low, the measured vitrinite reflectance was 0.54%, and the sample was determined to be an ideal thermal simulation sample.

When the gas leaves the gold tube under the internal pressure of 1×10^2 Pa and enters the vacuum equipment for gaseous compound analysis, large quantities of C_6 and C_7 compounds evaporate and are lost. Therefore, when the total amount of liquid hydrocarbon compounds produced was determined, only the amount of C_{8+} compounds was measured (Figure 10). At 2 °C/h and 20 °C/h, the maximum amounts of oil generated by the P_2l shale in the experiment were 209.2 mg/g (0.96EASY%Ro) and 172.3 mg/g (1.08EASY%Ro), respectively (Figure 10). There was no large difference in the maximum amount of oil generated by the sample at the heating rates of 2 °C/h and 20 °C/h. When EASY%Ro > 1.0, the maximum amount of oil generated at a heating rate of 2 °C/h was slightly higher than that generated at a heating rate of 20 °C/h (Figure 10). The experimental results show that the heating rate was not the key factor controlling the crude oil yield in this study. During the thermal simulation process, when the kerogen was cracked to produce crude oil for the first time, part of the crude oil was cracked to generate natural gas at the same time. Therefore, we could assume that the measured maximum amount of oil generated represented a conversion rate of 95% for the kerogen sample [42]. Based on this assumption, the maximum amount of oil generated by the sample in this study was 220.2 mg/g TOC (209.2 mg/g TOC/0.95).

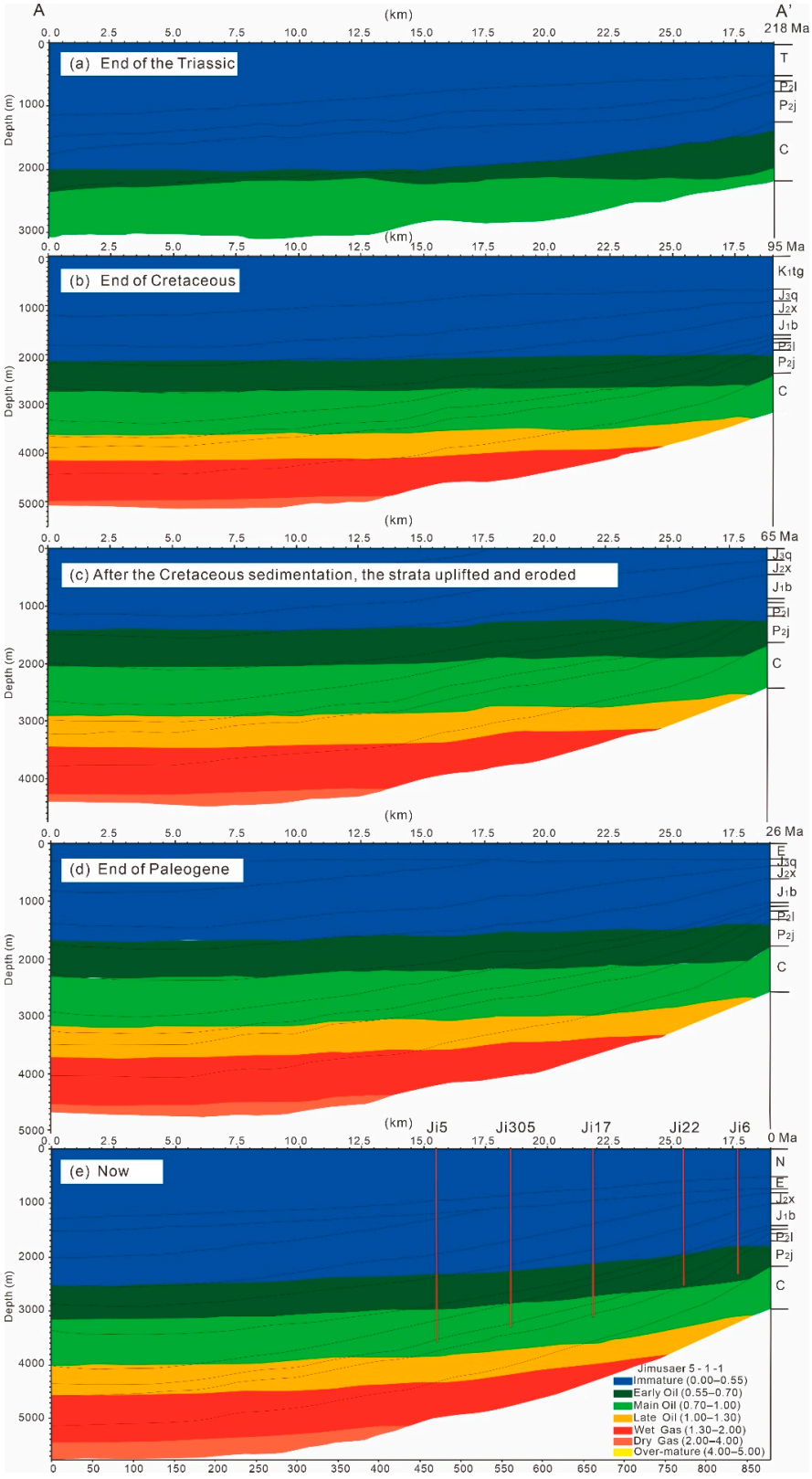

Figure 9. Two-dimensional simulation profile of the thermal evolution and burial history of the P_2l source rocks in the Jimsar Depression (Late Triassic (**a**); Late Cretaceous (**b**); after Cretaceous deposition, uplift and denudation of formations (**c**); Late Paleogene (**d**); present day(**e**)). The location of this section can be found in Figure 1c.

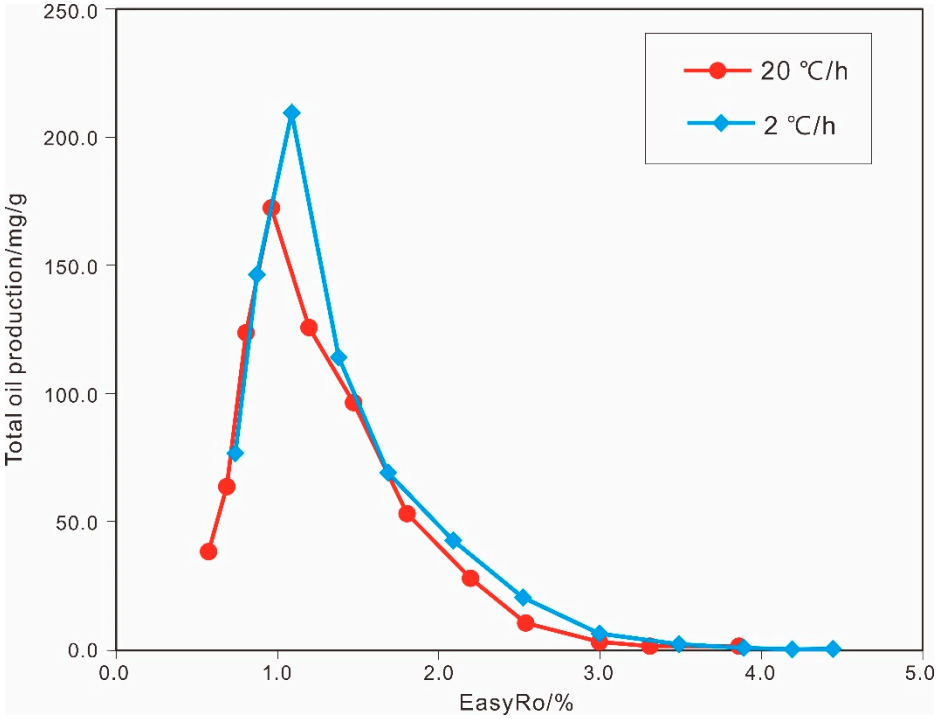

Figure 10. Simulation results of the oil production rate under different heating rates of the P_2l source rocks in the Jimsar Depression.

The organic adsorption model proposed by Pepper (1992) and Sandvik et al. (1992) [43,44] can be used to estimate the amount of oil expelled from the source rocks. We defined R as the amount of residual oil in g/g TOC, and we defined M and W as the final amount of oil generated and the final amount of oil expelled per gram of initial organic carbon in the source rocks, respectively [42]. Assuming that the carbon content of the expelled crude oil was 80% after the oil expulsion was completed, the amount of residual organic carbon and residual oil per gram of original organic carbon in the source rocks were $(1 - 0.8 \times W)$ and $R \times (1 - 0.8 \times W)$, respectively; thus, the following equations could be established [42]:

$$M = W + R \times (1 - 0.8 \times W), \quad (1)$$

$$W = (M - R)/(1 - 0.8 \times R), \quad (2)$$

where the units of M and W are g/g TOC. As previously mentioned, according to the pyrolysis experiment conducted in the closed system, the maximum amount of oil generated (M) by the sample was 220.2 mg/g TOC. The content (R) of bitumen extracted from the P_2l source rocks in the Jimsar Depression was mainly in the range of 60–100 mg/g, the maximum amount of expelled crude oil (W) was 130.7–168.2 mg/g TOC, and the maximum hydrocarbon expulsion efficiency was 59.3–76.4% [42,43,45].

5. Conclusions

Based on data from the hydrocarbon pyrolysis, the contents of organic carbon and soluble organic matter, the biomarkers, the organic microscopic composition, the vitrinite reflectance, the basin simulation and hydrocarbon generation experiments, the sedimentary environment, hydrocarbon generation capacity, quality, and maturity of the Lucaogou Formation were discussed. Four main conclusions could be drawn.

(1) The majority of the organic matter in the Lucaogou Formation came from algae, and the sedimentary water environment had high reducibility and salinity.
(2) The organic microscopic components of the Lucaogou source rocks were dominated by the sapropelinite group and exinite group, and they were a set of oil-prone source

rocks. Most of them were rated as good and extremely good, but their heterogeneity was strong.

(3) At the end of the Cretaceous period, the Lucaogou Formation source rocks entered the main oil generation window and began to generate a large amount of normal crude oil. Currently, the deep part of the depression has generally reached the high-maturity stage and is generating a large amount of highly mature oil and condensate gas. The maturity of the shallow part is relatively low, and only a large amount of conventional crude oil can be generated.

(4) The thermal simulation experiment conducted in a closed system suggests that the Lucaogou source rocks have great hydrocarbon generation capacity and expulsion efficiency, and the heating rate did not have a significant impact on the maximum amount of oil generated.

Author Contributions: Conceptualization, W.H., D.L. and G.L.; methodology, W.H.; software, D.W. and Y.L.; validation, Y.L.; formal analysis, G.L.; investigation, G.G.; resources, W.H. and L.H.; data curation, L.H. and Y.Q.; writing—original draft preparation, W.H. and Y.L.; writing—review and editing, Y.L.; visualization, D.W. and Y.L.; supervision, D.L. and G.L.; project administration, W.H.; funding acquisition, W.H. and Y.L. All authors have read and agreed to the published version of the manuscript.

Funding: This research was funded by the Strategic Priority Research Program of the Chinese Academy of Sciences (Grant No. XDA14010301), National Natural Science Foundation of China (Grant No. 41702138).

Institutional Review Board Statement: Not applicable.

Informed Consent Statement: Not applicable.

Data Availability Statement: Not applicable.

Acknowledgments: We want to thank the Xinjiang Oilfield Company for the support in preparing this manuscript. We also thank the editors and anonymous reviewers for their helpful suggestions and comments.

Conflicts of Interest: The authors declare no conflict of interest.

References

1. Bai, H.; Pang, X.Q.; Kuang, L.C.; Pang, H.; Wang, X.L.; Jia, X.Y.; Zhou, L.M.; Hu, T. Hydrocarbon expulsion potential of source rocks and its influence on the distribution of lacustrine tight oil reservoir, Middle Permian Lucaogou Formation, Jimsar Sag, Junggar Basin, Northwest China. *J. Pet. Sci. Eng.* **2017**, *149*, 740–755. [CrossRef]
2. Chen, Z.H.; Cao, Y.C.; Ma, Z.J.; Zhen, Y.S. Geochemistry and origins of natural gases in the Zhongguai area of Junggar Basin, China. *J. Pet. Sci. Eng.* **2014**, *119*, 17–27. [CrossRef]
3. Su, Y.; Zha, M.; Liu, K.Y.; Ding, X.J.; Qu, J.X.; Jin, J.H. Characterization of Pore Structures and Implications for Flow Transport Property of Tight Reservoirs: A Case Study of the Lucaogou Formation, Jimsar Sag, Junggar Basin, Northwestern China. *Energies* **2021**, *14*, 1251. [CrossRef]
4. Jiang, Y.H.; Hou, D.J.; Li, H.; Zhang, Z.M.; Guo, R.B. Impact of the Paleoclimate, Paleoenvironment, and Algae Bloom: Organic Matter Accumulation in the Lacustrine Lucaogou Formation of Jimsar Sag, Junggar Basin, NW China. *Energies* **2020**, *13*, 1488. [CrossRef]
5. Tang, Y.; Cao, J.; He, W.J.; Shan, X.; Liu, Y.; Zhao, K.B. Development Tendency of Geological Theory of Total Petroleum System: Insights from the Discovery of Mahu Large Oil Province. *Xinjiang Pet. Geol.* **2021**, *42*, 1–9, (In Chinese with English abstract).
6. Jia, C.Z.; Zou, C.N.; Li, J.Z.; Li, D.H.; Zheng, M. Assessment criteria, main types, basic features and resource prospects of the tight oil in China. *Acta Pet. Sin.* **2012**, *33*, 343–350, (In Chinese with English abstract).
7. Zou, C.N.; Yang, Z.; Tao, S.Z.; Yuan, X.J.; Zhu, R.K.; Hou, L.H.; Wu, S.T.; Sun, L.; Zhang, G.S.; Bai, B.; et al. Continuous hydrocarbon accumulation over a large area as a distinguishing characteristic of unconventional petroleum; the Ordos Basin, north-central China. *Earth-Sci. Rev.* **2013**, *126*, 358–369. [CrossRef]
8. Zou, C.N.; Zhu, R.K.; Bai, B.; Yang, Z.M.; Hou, L.H.; Zha, M.; Fu, J.H.; Shao, Y.; Liu, K.Y.; Cao, H.; et al. Significance, Geologic Characteristics, Resource Potential and Future Challenges of Tight Oil and Shale Oil. *Bull. Mineral. Petrol. Geochem.* **2015**, *34*, 3–17, (In Chinese with English abstract).
9. Katz, B.; Lin, F. Lacustrine basin unconventional resource plays: Key differences. *Mar. Pet. Geol.* **2014**, *56*, 255–265. [CrossRef]

10. Carroll, A.R. Upper Permian lacustrine organic facies evolution, southern Junggar Basin, NW China. *Org. Geochem.* **1998**, *28*, 649–667. [CrossRef]
11. Jiang, Y.Q.; Liu, Y.Q.; Yang, Z.; Nan, Y.; Wang, R.; Zhou, P.; Yang, Y.J.; Kou, J.Y.; Zhou, N.C. Characteristics and origin of tuff-type tight oil in Jimusar Depression, Junggar Basin, NW China. *Pet. Explor. Dev.* **2015**, *42*, 741–749, (In Chinese with English abstract). [CrossRef]
12. Wang, Y.T.; Yang, Z.M.; Ma, W.C.; Pan, C.C.; Wang, F. Geochemical Characteristics and Genesis of Tight Oil in Lucaogou Formation of Jimsar Sag. *Xinjiang Pet. Geol.* **2017**, *38*, 379–384, (In Chinese with English abstract).
13. Hu, T.; Pang, X.Q.; Jiang, S.; Wang, Q.F.; Zheng, X.W.; Ding, X.G.; Zhao, Y.; Zhu, C.X.; Li, H. Oil content evaluation of lacustrine organic-rich shale with strong heterogeneity: A case study of the Middle Permian Lucaogou Formation in Jimusaer Sag, Junggar Basin, NW China. *Fuel* **2018**, *221*, 196–205. [CrossRef]
14. Kuang, L.C.; Wang, X.T.; Guo, X.G.; Chang, Q.S.; Jia, X.Y. Geological Characteristics and Exploration Practice of Tight Oil of Lucaogou Formation in Jimsar Sag. *Xinjiang Pet. Geol.* **2015**, *36*, 629–634, (In Chinese with English abstract).
15. Gao, G.; Xiang, B.L.; Li, T.T.; Ren, J.L.; Kong, Y.H. Tight Oil System Particularity of Lucaogou Formation in Jimusaer Sag, Junggar Basin. *Acta Sedimentol. Sin.* **2017**, *35*, 824–833, (In Chinese with English abstract).
16. Wang, X.L.; Zhi, D.M.; Wang, Y.T.; Chen, J.P.; Qin, Z.J.; Liu, D.G.; Xiang, Y.; Lan, W.F.; Li, N. *Organic Geochemistry of Source Rocks and Hydrocarbons in the Junggar Basin*; Petroleum Industry Press: Beijing, China, 2013; pp. 18–73. (In Chinese)
17. Wu, H.G.; Hu, W.X.; Tang, Y.; Cao, J.; Wang, X.L.; Wang, Y.C.; Kang, X. The impact of organic fluids on the carbon isotopic compositions of carbonate-rich reservoirs: Case study of the Lucaogou Formation in the Jimusaer Sag, Junggar Basin, NW China. *Mar. Pet. Geol.* **2017**, *85*, 136–150. [CrossRef]
18. Shao, Y.; Yang, Y.Q.; Wan, M.; Qiu, L.W.; Cao, Y.C.; Yang, S.C. Sedimentary Characteristic and Facies Evolution of Permian Lucaogou Formation in Jimsar Sag, Junggar Basin. *Xinjiang Pet. Geol.* **2015**, *36*, 635–641, (In Chinese with English abstract).
19. Hou, L.H.; Zou, C.N.; Liu, L.; Wen, B.H.; Wu, X.Z.; Wei, Y.Z.; Mao, Z.G. Geologic essential elements for hydrocarbon accumulation within Carboniferous volcanic weathered crusts in northern Xinjiang, China. *Acta Pet. Sin.* **2012**, *33*, 533–540, (In Chinese with English abstract).
20. Kuang, L.C.; Hu, W.X.; Wang, X.L.; Wu, H.G.; Wang, X.L. Research of the Tight Oil Reservoir in the Lucaogou Formation in Jimusar Sag: Analysis of Lithology and Porosity Characteristics. *Geol. J. China Univ.* **2013**, *19*, 529–535, (In Chinese with English abstract).
21. Cao, Z.; Liu, G.D.; Kong, Y.H.; Wang, C.Y.; Niu, Z.C.; Zhang, J.Y.; Geng, C.B.; Shan, X.; Wei, Z.P. Lacustrine tight oil accumulation characteristics: Permian Lucaogou Formation in Jimusaer Sag, Junggar Basin. *Int. J. Coal Geol.* **2016**, *153*, 37–51. [CrossRef]
22. Wang, S.J.; Hu, S.B.; Li, T.J.; Wang, J.Y.; Zhao, W.Z. Terrestrial heat flow in Junggar Basin, Northwest China. *Chin. Sci. Bull.* **2000**, *45*, 1327–1332, (In Chinese with English abstract). [CrossRef]
23. Wang, S.J.; Hu, S.B.; Wang, J.Y. The Characteristics of heat flow and geothermal fields in Junggar Basin. *Chin. J. Geophys.* **2000**, *43*, 771–779, (In Chinese with English abstract). [CrossRef]
24. Sweeney, J.J.; Burnham, A.K. Evaluation of a Simple Model of Vitrinite Reflectance Based on Chemical Kinetics. *AAPG Bull.* **1990**, *74*, 1559–1570.
25. Peters, K.E.; Walters, C.C.; Moldowan, J.M. *The Biomarker Guide: Interpreting Molecular Fossils in Petroleum and Ancient Sediments*; Cambridge University Press: Cambridge, UK, 2005; pp. 1–1155.
26. Powell, T.G. Pristane/phytane ratio as environmental indicator. *Nature* **1988**, *333*, 604. [CrossRef]
27. Shanmugan, G. Significance of coniferous rain forests and related oil, Gippsland Basin, Australia. *AAPG Bulletin* **1985**, *69*, 1241–1254.
28. Vu, T.T.A.; Zink, K.G.; Mangelsdorf, K.; Sykes, R.; Wilkes, H.; Horsfield, B. Changes in bulk properties and molecular compositions within New Zealand Coal Band solvent extracts from early diagenetic to catagenetic maturity levels. *Org. Geochem.* **2009**, *40*, 963–977. [CrossRef]
29. Azevedo, D.A.; Aquino Neto, F.R.; Simoneit, B.R.T.; Pinto, A.C. Novel series of tricyclic aromatic terpanes characterized in Tasmanian tasmanite. *Org. Geochem.* **1992**, *18*, 9–16. [CrossRef]
30. Ourisson, G.; Albrecht, P.; Rohmer, M. The hopanoids, paleochemistry and biochemistry of a group of natural products: Pure Applied Chemistry. *Pure Appl. Chem.* **1979**, *51*, 709. [CrossRef]
31. Damsté, J.S.S.; Duin, A.; Hollander, D.; Kohnen, M.E.L.; Leeuw, J.W.D. Early diagenesis of bacteriohopanepolyol derivatives: Formation of fossil homohopanoids. *Geochim. Cosmochim. Acta* **1995**, *59*, 5141–5157. [CrossRef]
32. Ten Haven, H.L.; De Leeuw, J.W.; Sinninghe, D.J.S.; Schenck, P.A.; Palmer, S.E.; Zumberge, J.E. Application of Biological Markers in the Recognition of Palaeohypersaline Environments. In *Lacustrine Petroleum Source-Rocks*; Fleet, A.J., Kelts, K., Talbot, M.R., Eds.; Geological Society Special Publication: Oxford, UK, 1988; Volume 40, pp. 123–130.
33. Schwark, L.; Empt, P. Sterane biomarkers as indicators of palaeozoic algal evolution and extinction events. *Palaeogeogr. Palaeoclimatol. Palaeoecol* **2006**, *240*, 225–236. [CrossRef]
34. Moldowan, J.M.; Seifert, W.K.; Gallegos, E.J. Relationship between Petroleum Composition and Depositional Environment of Petroleum Source Rocks1. *AAPG Bull.* **1985**, *69*, 1255–1268.
35. Dai, J.X. *Large Coal-Formed Gas Fields and Gas Sources in China*; Science Press: Beijing, China, 2017; pp. 1–454. (In Chinese)
36. Gong, D.Y.; Lan, W.F.; Xiang, H.; Ding, J.; Wu, W.A.; Hu, Z.L. Genetic types and origins of natural gases from the eastern Junggar basin. *J. China Univ. Min. Technol.* **2019**, *48*, 142–152, (In Chinese with English abstract).

37. Hunt, J.M. *Petroleum Geology and Geochemistry*; Freeman Company: San Francisco, CA, USA, 1996.
38. Tissot, B.P.; Welte, D.H. *Petroleum Formation and Occurrence*; Springer: Berlin/Heidelberg, Germany; New York, NY, USA, 1984; pp. 1–699.
39. Bordenave, M.L. *Applied Petroleum Geochemistry*; Editions Technip: Paris, France, 1993; pp. 344–353.
40. Huang, D.F.; Li, J.C. *Continental Hydrocarbon Generation in China*; Petroleum Industry Press: Beijing, China, 1982; pp. 1–355. (In Chinese)
41. Peters, K.E. Guidelines for Evaluating Petroleum Source Rock Using Programmed Pyrolysis1. *AAPG Bulletin* **1986**, *70*, 318–329.
42. Xiang, B.L.; Li, E.T.; Gao, X.W.; Wang, M.; Wang, Y.; Xu, H.; Huang, P.; Yu, S.; Liu, J.Z.; Zou, Y.R.; et al. Petroleum generation kinetics for Permian lacustrine source rocks in the Junggar Basin, NW China. *Org. Geochem.* **2016**, *98*, 1–17. [CrossRef]
43. Pepper, A.S. Estimating of Petroleum Expulsion Behavior of Source Rocks: A Novel Quantitative Approach. In *Petroleum Migration*; England, A.J., Fleet, A.J., Eds.; Geological Society Special Publication: London, UK, 1992; Volume 59, pp. 9–31.
44. Sandvik, E.I.; Young, W.A.; Curry, D.J. Expulsion from hydrocarbon sources: The role of organic absorption. *Org. Geochem.* **1992**, *19*, 77–87. [CrossRef]
45. Cooles, G.P.; Mackenzie, A.S.; Quigley, T.M. Calculation of petroleum masses generated and expelled from source rocks. *Org. Geochem.* **1986**, *10*, 235–245. [CrossRef]